ACS APPLIED ELECTRONIC MATERIALS

Article

Cite This: ACS Appl. Electron. Mater. 2019, 1, 210−219

pubs.acs.org/acsaelm

Contact Engineering for Dual-Gate MoS_2 Transistors Using O_2 Plasma Exposure

Pavel Bolshakov,[†] Christopher M. Smyth,[†] Ava Khosravi,[†] Peng Zhao,[†] Paul K. Hurley,[‡] Christopher L. Hinkle,[†] Robert M. Wallace,[†] and Chadwin D. Young*[,†]

[†]Department of Materials Science and Engineering, The University of Texas at Dallas, 800 West Campbell Road, Richardson, Texas 75080, United States

[‡]Tyndall National Institute, University College Cork, Lee Maltings Complex, Dyke Parade, Mardyke, Cork, Ireland

Supporting Information

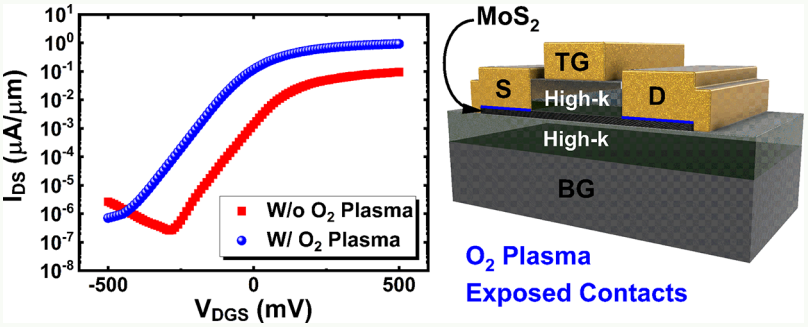

ABSTRACT: The benefits of O_2 plasma exposure at the contact regions of dual-gate MoS_2 transistors prior to metal deposition for high performance electron contacts are studied and evaluated. Comparisons between devices with and without the exposure demonstrate significant improvements due to the formation of a high-quality contact interface with low electron Schottky barrier (~0.1 eV). Topographical and interfacial characterizations are used to study the contact formation on MoS_2 from the initial exfoliated surface through the photolithography process and Ti deposition. Fermi level pinning near the conduction band is shown to take place after photoresist development leaves residue on the MoS_2 surface. After O_2 plasma exposure and subsequent Ti deposition, Ti scavenges oxygen from MoO_x and forms TiO_x. Electrical characterization results indicate that photoresist residue and other contaminants present after development can significantly impact electrical performance. Without O_2 plasma exposure at the contacts, output characteristics of MoS_2 FETs demonstrate nonlinear, Schottky-like contact behavior compared to the linearity observed for contacts with exposure. O_2 plasma allows for the removal of the residue present at the surface of MoS_2 without the use of a high-temperature anneal. A low conduction band offset and superior carrier injection are engineered by employing the reactive metal Ti as the contact to deliberately form TiO_2. Dual-gate MoS_2 transistors with O_2 plasma exposure at the contacts demonstrate linear output characteristics, lower contact resistance (~20× reduction), and higher field effect mobility (~15× increase) compared to those without the treatment. In addition, these results indicate that device fabrication process induced effects cannot be ignored during the formation of contacts on MoS_2 and other 2D materials.

KEYWORDS: *MoS_2, MOSFETs, contacts, O_2 plasma, contact resistance, TiO_2, photoresist residue*

I. INTRODUCTION

Transitional metal dichalcogenides (TMDs) are a group of 2D materials with the potential to act as the channel material in low-power, high mobility devices.[1−3] For nearly a decade, significant strides have been made in understanding the intriguing electrical and optical properties of 2D TMDs. From semimetals, semiconductors (e.g., MoS_2 and WSe_2), and superconductors (e.g., NbS_2 and $NbSe_2$), among others, TMDs have an array of potential uses in a myriad of useful applications such as 2D photodetectors, solar cells, and transistors.[4,5] Furthermore, the layered nature of TMDs presents a number of potential applications for any single material where a direct band gap (layer # $N = 1$), ideal for optoelectronics, and an indirect band gap ($N > 1$) would allow the implementation of LEDs and thin-film transistors using the same TMD material.[3,6] The fascinating properties do not stop there, as different phases of a material, MoS_2 for example, can be either metallic (1T-MoS_2) or semiconducting (2H-MoS_2), allowing for even greater flexibility in the use of and exploitation of TMDs.[7] It is therefore important to be able to fabricate a large scale of TMD devices with low variability, high uniformity, and efficient electrical performance to study the aforementioned properties in greater detail.

Received: November 13, 2018
Accepted: January 17, 2019
Published: January 17, 2019

DOI: 10.1021/acsaelm.8b00059
ACS Appl. Electron. Mater. 2019, 1, 210−219

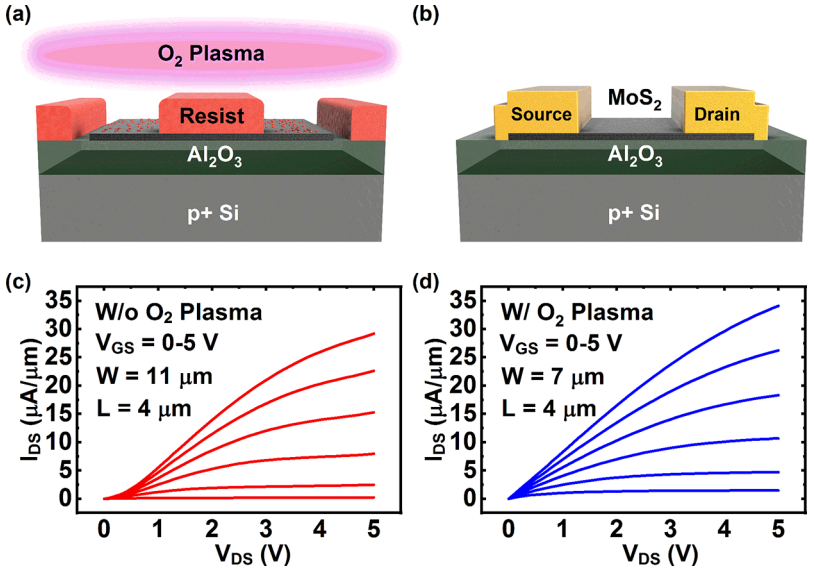

Figure 1. (a) Graphic illustrating the O_2 plasma exposure at the exposed contact areas after development of the photoresist and (b) the final back-gate MoS_2 FET structure. (c) Output characteristics of MoS_2 FET without O_2 plasma exposure demonstrating nonlinear I_{DS}–V_{DS} and (d) with O_2 plasma exposure demonstrating a more linear I_{DS}–V_{DS}.

A major stopgap that has plagued TMD devices has been the high contact resistance (R_C) at the source and drain contacts.[8,9] The current state of contacts on TMDs is susceptible to the Fermi level pinning (FLP) effect, where the Schottky barrier height (SBH) does not follow the Schottky–Mott rule, suggesting a metal work function independent of R_C.[10,11] Experimental studies comparing contact metals on MoS_2 show significant disparities on which metal provides the best contact interface.[12,13] Furthermore, using several low and high work function metals (Sc, Ti, Ni, and Pt) as contacts on MoS_2, for example, results in n-type behavior irrespective of the metal used, suggesting that the contact metal is not the major contributor to the FLP near the conduction band.[12] This discrepancy between the predicted theoretical device behavior and experimental studies must be understood to help eliminate the FLP and reduce the R_C. Additionally, there are differences in device behaviors for different research groups that use the same TMD/contact metal interface for their devices. This can be attributed to differences in processing, metal deposition conditions, and source of the TMD, among other factors.[14,15] Understanding the role of such processing conditions on TMDs is important in narrowing down the deciding factor(s) responsible for such discrepancies and their contribution, if any, to the FLP effect and the high R_C.

The role of TMD flake thickness has also been determined to substantially affect device performance and R_C. Monolayer and bilayer thick TMD flakes demonstrate R_C values significantly higher than bulk samples ($N > 2$). Several reports have shown few-layer MoS_2 flakes beyond five or more layers exhibit better device performance and lower R_C values than their monolayer and bilayer counterparts.[12,16] Das et al. have even shown there also exists an upper limit as well, suggesting that to extract the best device performance out of MoS_2 flakes, a thickness in the range of 6–12 nm would be optimal.[12] Great care must be taken when comparing any two devices, ensuring TMD flake thickness and device dimensions are very similar.

Current large-scale semiconductor manufacturing uses a photolithographic process, suggesting this will be the method of choice for implementation of high-volume manufacturing of TMD devices, given the low throughput of electron-beam lithography (EBL), which has been used substantially in fabrication of TMD devices for research purposes. A major component that is common to most TMD studies involving devices is the use of photoresist during fabrication. Often, a high-temperature anneal is used to "clean" photoresist residue and other contaminants present after device processing from interfaces within a device.[14,17,18] This is not ideal because reactions at the contact metal/MoS_2 interface may take place during such anneals, which can degrade contact performance in some cases. The dielectric and the MoS_2 may also be affected by such anneals, which can convolute the interpretations of the electrical device characteristics. More recently, using contact mode atomic force microscopy (AFM) to remove residue has been suggested as another potential option.[19] Although it can be useful for proof of concept, it is not a scalable method for high-volume manufacturing. Industry commonly employs a plasma step after photoresist development in traditional lithography processes on Si to remove any photoresist residue before further processing.[20] The same concept may be applied to TMDs, such as MoS_2, for the same specific purpose. It is important to note that the underlying material, MoS_2, is fundamentally an ultrathin body semiconductor compared to bulk Si. Thus, certain considerations must be weighed: the role of photoresist residue on the electrostatics of MoS_2, the surface reactions, if any, as a result of the O_2 plasma exposure, and if there is substantial etching of the MoS_2 layers. It is also prudent to comment on previous studies involving the use of O_2 plasma on MoS_2, which focused on either the functionalization of MoS_2 for deposition of thin, pinhole free high-k dielectrics,[21] or layer-by-layer etching of MoS_2,[22] or O_2 plasma exposure at the MoS_2 channel region for overall improvement in device performance.[23,24] The technique used in this study consists of a short, low-power, direct O_2 plasma exposure to etch away the photoresist residue and functionalize the MoS_2 contact surface for controlled interface chemistry.

DOI: 10.1021/acsaelm.8b00059
ACS Appl. Electron. Mater. 2019, 1, 210–219

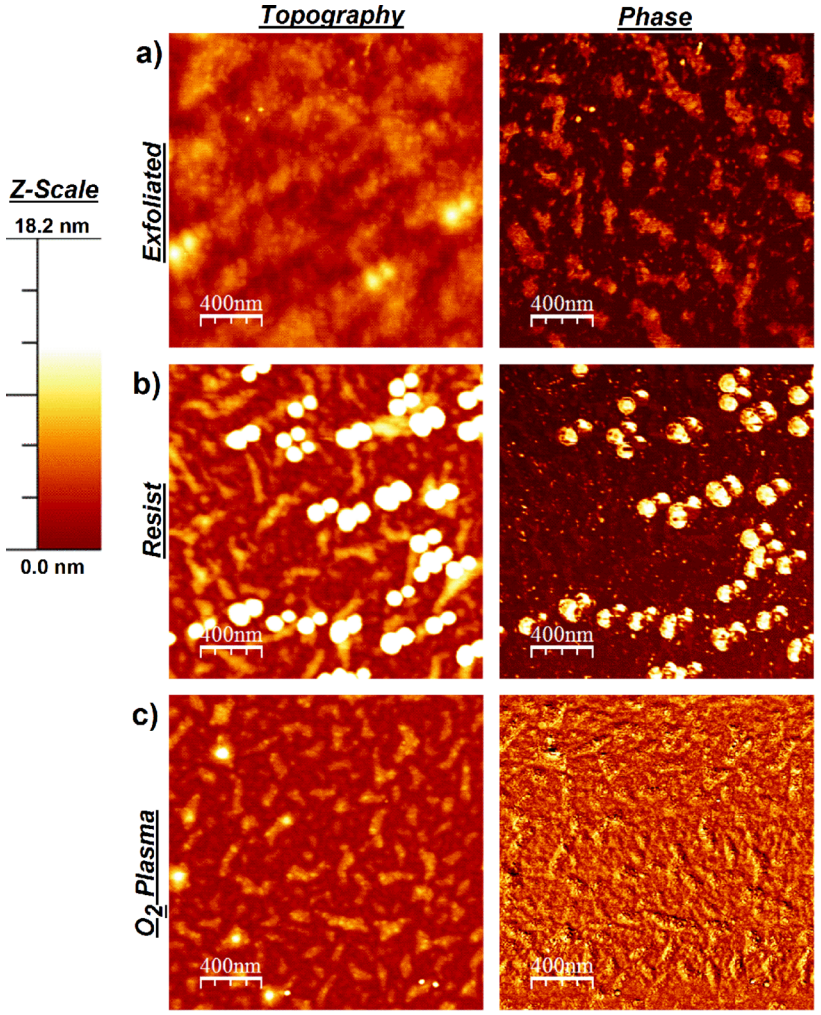

Figure 2. AFM topography and phase images obtained from a MoS_2 flake after (a) exfoliation, (b) photolithography processing (photoresist deposition, exposure, and development), and (c) O_2 plasma exposure.

Using a 5 s O_2 plasma exposure prior to Ti contact metal deposition results in the formation of a high-quality metal/MoS_2 contact interface due to the formation of TiO_2. The dual purpose of O_2 plasma exposure to remove photoresist residue and functionalize the contact areas for TiO_2 formation serves to depin the Fermi level from near the conduction band and reduce overall R_C. A systematic study of contact formation, which is exhibited through the use of electrical, topographical, and chemical analysis, provides insights into the role photoresist residue has on MoS_2 devices. The correlation between physical and the electrical characterization is done to understand the impact of process induced contaminants on device performance. Valence band edge extraction appears to demonstrate FLP near the conduction band edge with the introduction of photoresist residue, suggesting it may be the major factor behind the FLP effect observed in TMD devices. Dual-gate MoS_2 FETs with and without the O_2 plasma exposure at the contacts are compared and demonstrate a reduction in contact resistance (R_C) of ~20× as well as an ~15× increase in field effect mobility (μ_{FE}). This process has the potential to be extended to other TMDs and 2D materials to improve the contact metal interface and achieve superior device characteristics for many device applications.

II. EXPERIMENTAL SECTION

Al_2O_3 (~27 nm for optical contrast and rapid MoS_2 flake identification[25]) was deposited by atomic layer deposition (ALD) at 250 °C onto a p^{++}Si wafer (post-RCA clean) for back-gate (BG) isolation. On the opposite side of the Si wafer, Al was deposited for a backside wafer contact followed by a 400 °C forming gas anneal to remove charges present in the Al_2O_3 following the 250 °C ALD growth. The ALD Al_2O_3 on the p^{++}Si then serves as the "substrate", and the Al_2O_3 serves as a BG oxide for exfoliated multilayer, synthetic[26] MoS_2 flakes.[27,28] By use of photolithography, with AZ nLOF 2020 negative photoresist along with AZ 300 MiF developer,[29] source/drain contacts are defined on the transferred flake (~4−8 nm thickness) followed by a 5 s O_2 plasma exposure ("descum") at 50 W and 200 mTorr (base pressure <5 mTorr) to remove photoresist residue prior to contact metal deposition on MoS_2 (see Figure 1a,b). Immediately after, Ti/Au (10 nm/140 nm) is deposited using e-beam evaporation in high vacuum (base pressure $<5 \times 10^{-6}$ mbar) followed by a lift-off process. Electrical BG measurements are then performed followed by a 300 °C UHV anneal for 2 h to facilitate desorption of residual contaminants.[30,31] Then, a 15 min *in situ*, room-temperature UV-ozone surface treatment is performed followed by Al_2O_3/HfO_2 (3 nm/6 nm) deposition at 200 °C using ALD for top high-κ gate dielectric formation.[32,33] The high-κ dielectric deposition is followed by photolithography patterning and metallization of a Pd/Au (20/140 nm) top-gate to produce $p^{++}Si/Al_2O_3/MoS_2/Al_2O_3/HfO_2$/Pd/Au dual-gate structures. The structures are electrically characterized with

DOI: 10.1021/acsaelm.8b00059
ACS Appl. Electron. Mater. 2019, 1, 210−219

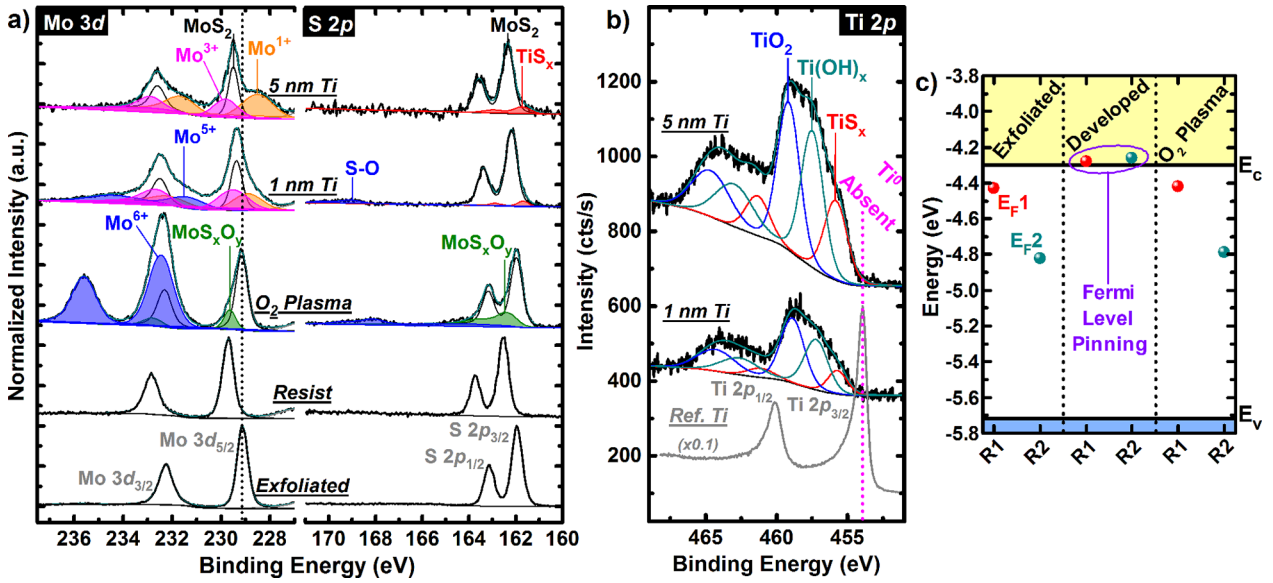

Figure 3. XPS core level spectra ((a) Mo 3d, S 2p and (b) Ti 2p) obtained from bulk MoS_2 after exfoliation, typical photolithographic processing (deposition, exposure, and development), 5 s O_2 plasma, 1 nm Ti deposition, and 5 nm Ti deposition. These spectra show MoO_x forms on MoS_2 during O_2 plasma. Ti deposited during subsequent metallization reduces MoO_x and reacts with MoS_2 forming TiO_x and TiS_x at the Ti/MoS_2 interface. The spectra in (a) and (b) were obtained in the same experiment from the same MoS_2 crystal. The Ti thicknesses listed reflect the total film thickness. (c) Band alignment of two bulk MoS_2 crystals after exfoliation and photolithographic processing: according to the measured valence band offset and expected bulk MoS_2 band gap, Fermi level pinning is occurring in bulk MoS_2 after photolithographic processing.

a dual-gate sweeping methodology[34,35] using a Keithley 4200 Semiconductor Characterization System in a Cascade Probe Station.

Atomic force microscope (AFM) images were obtained *ex situ* from MoS_2 flakes after exfoliation, development, and descum with a Veeco Model 3100 Dimension V atomic probe microscope in noncontact tapping mode. Images were processed using the WSxM software.[32]

The surface chemistry of a bulk, geological MoS_2 crystal from 2D Semiconductors[26] was investigated with X-ray photoelectron spectroscopy (XPS) *ex situ* after exfoliation, development, and descum. After descum and XPS, Ti was deposited *in situ* in a separate deposition chamber attached to a cluster tool described elsewhere.[36] This was done consecutively in two steps to obtain total thickness values of 1 and 5 nm, while XPS was performed *in situ* after each deposition step without breaking vacuum ($<2 \times 10^{-9}$ mbar) in an analysis chamber attached to the same cluster tool. Prior to Ti deposition on MoS_2, the Ti metal source was prepared, and the deposition rate was determined to be identical with that previously employed in similar experiments.[15,37] Before Ti metallization, the deposition chamber, which was initially held at a base pressure of $<2 \times 10^{-9}$ mbar, was backfilled with air. The flow rate was adjusted to maintain a pressure of 5×10^{-6} mbar throughout Ti deposition to simulate the environment commonly found in an elastomer-sealed deposition chamber, which was employed in the device fabrication process performed in this work.

XPS analysis was performed via a monochromated Al Kα X-ray source ($h\nu$ = 1486.7 eV) and an Omicrometer EA125 Hemispherical Analyzer with ±0.05 eV resolution. High-resolution spectra were obtained at a takeoff angle of 45°, acceptance angle of 8°, and pass energy of 15 eV. The analyzer was calibrated with polycrystalline Au, Ag, and Cu foils according to ASTM E2108.[38] Spectra were deconvolved with AAnalyzer, a peak fitting software.[39]

III. RESULTS AND DISCUSSION

One of the major advantages of using a plasma clean at the contact regions is that it is performed prior to the formation of the metal/MoS_2 interface. A high-temperature thermal anneal post-development and prior to metallization with enough energy to drive off the photoresist residue and other contaminants would damage the surrounding photoresist. When using a 5 s O_2 plasma exposure, the exposed contact regions are cleaned while the rest of the MoS_2, which serves as the channel, is protected by a 2 μm thick photoresist layer as shown in Figure 1a. Several back-gated MoS_2 FETs were fabricated (see Figure S1 in the Supporting Information for a thorough photolithography flow diagram) with and without the O_2 plasma exposure to compare the electrical response (Figure 1b). The output characteristics of a transistor with Ti/Au contacts, where Ti serves as the interfacial contact metal,[40] without O_2 plasma show nonlinearity (Figure 1c). With the inclusion of the plasma exposure, the output characteristics become "Ohmic-like" as shown in Figure 1d. The linearity of $I_{DS}-V_{DS}$ curves, as well as an overall reduction in device-to-device performance variability, is consistently observed in multiple MoS_2 FETs with O_2 plasma exposure and Ti/Au contacts (see Figure S2). Previous studies that utilize O_2 plasma on MoS_2 used it either as a functionalization treatment for deposition of uniform, pinhole-free dielectric films or for layer-by-layer etching.[21,22]

The major side effect of O_2 plasma exposure is the formation of MoO_x byproducts on the MoS_2 surface. MoO_x exhibits a high electron affinity and work function (up to ~6.5 eV),[41] leading to formation of a p-type contact ideal for hole injection in MoS_2 FETs.[42,43] This would suggest that O_2 plasma exposure at the contact areas on MoS_2 prior to metal deposition would lead to the formation of p-type contacts, resulting in severe nonlinearity in the n-channel MoS_2 output characteristics, as opposed to the reduced contact resistance which is observed experimentally (Figure 1d). Spectroscopic and topographic investigations were performed on MoS_2 at all major contact formation steps in the device fabrication process to understand the n-type contact behavior.

By use of atomic force microscopy (AFM), the surface topography and phase of few-layer MoS_2 flakes after exfoliation, development, and O_2 plasma exposure are investigated to ascertain the amount of photoresist residue

DOI: 10.1021/acsaelm.8b00059
ACS Appl. Electron. Mater. 2019, 1, 210−219

after development and its removal during O_2 plasma. After exfoliation and transfer of MoS_2 on to the Al_2O_3/Si substrate, the initial surface topography and phase are depicted in Figure 2a. A relatively rough surface is detected (rms roughness = 1.43 nm), potentially due to stresses induced during the exfoliation and transfer process. Nonetheless, multiple few-layer MoS_2 flakes on the Al_2O_3/Si substrate investigated with AFM in this work exhibit similar surface topography to that shown in Figure 2a. Following initial AFM, the photolithography process was performed on the MoS_2 to form the contact areas. Large islands (up to 20 nm in height and 50 nm in diameter), lower profile wrinkle-like features, and significant increase in rms roughness (6.27 nm) are detected in AFM images after development (Figure 2b), which indicates a substantial amount of photoresist residue is left behind after lift-off. This suggests the resist residue will cause discontinuous contact between an adhesion layer often employed in contacts to TMDs, such as Ti,[44,45] and the underlying TMD, which likely convolutes the electrical response of analogous contacts. The AFM images displayed in Figure 2c show the MoS_2 surface after 5 s O_2 plasma exposure. Large clusters present after development are effectively removed during this step. However, lower profile, wrinkle-like features remain, which could correspond with either small areas of resist residue or patches of MoO_x. Nonetheless, the rms roughness after O_2 plasma (1.39 nm) is comparable to that of the exfoliated MoS_2. This demonstrates that a short O_2 plasma step after development is enough to remove a majority of the organic residue prior to metal deposition. It is also important to note that the thickness of the multilayer MoS_2 flakes is not altered appreciably by the development process or the subsequent O_2 plasma process, which indicates the treatment may be compatible with monolayer MoS_2 (see Figure S3 and associated discussion in the Supporting Information for more details).

Using X-ray photoelectron spectroscopy (XPS), we investigated the MoS_2 surface chemistry after exfoliation, development, and Ti deposition in high vacuum (HV, base pressure 5×10^{-6} mbar) to total thicknesses of 1 and 5 nm to elucidate the effects of resist residue and O_2 plasma on the Ti/MoS_2 interface chemistry.[40]

The Mo 3d and S 2p core level spectra obtained from bulk MoS_2 are shown in Figure 3a after each of the major processing steps defined above. The Mo $3d_{5/2}$ and $3d_{3/2}$ core levels are detected from exfoliated MoS_2 at binding energies of 229.1 and 232.2 eV, respectively, while the S $2p_{3/2}$ and $2p_{1/2}$ core levels are detected at binding energies of 161.9 and 163.1 eV, respectively. Initially, the valence band edge resides 0.9 eV from the Fermi level (Figure S4a). After photoresist deposition and development, the MoS_2 chemical states shift to higher binding energy (BE) by 0.6 eV, which indicates a Fermi level shift of equal magnitude toward the conduction band (E_C) edge. Considering the ~1.4 eV band gap of bulk MoS_2, the initial 0.9 eV valence band offset, and the 0.6 eV Fermi level shift after development, the Fermi level is pinned at the E_C edge by the photoresist residue (Figure 3c and Figure S4).[46] The same experiment was performed on a second bulk, geological MoS_2 crystal to investigate the consistency of Fermi level pinning (FLP) across different samples. The second exfoliated crystal exhibits a valence band edge 1.3 eV from the Fermi level and shifts ~0.2 eV after development, which is consistent with FLP at the E_C edge in agreement with the first crystal (Figure 3c and Figure S4). This demonstrates photoresist residue pins the Fermi level at roughly the same energy relative to the band edges regardless of the initial Fermi level position. Photoresist residue-induced FLP near the MoS_2 E_C edge could explain why it is so difficult to form p-type contacts on MoS_2.[47] After the O_2 plasma exposure, the MoS_2 chemical states in the Mo 3d and S 2p spectra shift back to the binding energies detected on exfoliated MoS_2. In addition, O_2 plasma causes significant oxidation of MoS_2 forming MoO_x (Mo^{6+}, 232.4 eV in the corresponding Mo $3d_{5/2}$ spectrum) and MoS_xO_y (229.6 and 162.4 eV in the corresponding Mo $3d_{5/2}$ and S $2p_{3/2}$ spectra, respectively). Therefore, the combination of hole injection by MoO_x and organic residue removal causes the Fermi level shift toward the valence band edge after O_2 plasma.

The MoS_xO_y chemical state in the Mo 3d and S 2p core levels is distinguishable from the Mo_xS_y chemical state detected in the Mo 3d and S 2p core levels in our previous work[40] after depositing Ti on MoS_2 *in situ* in UHV. The MoS_xO_y chemical state detected in this work in the Mo 3d core level after O_2 plasma exposure exhibits a higher BE than the MoS_2 chemical state, unlike the Mo_xS_y chemical state detected in the Mo 3d core level in our previous work, which exhibits a smaller BE than the MoS_2 chemical state. The O_2 plasma exposure oxidizes the MoS_2, substituting some sulfur atoms with oxygen atoms, resulting in the formation of the MoS_xO_y species. The oxygen is more electronegative than sulfur by 0.86 according to the Pauling electronegativity scale.[48] Therefore, the formation of a MoS_xO_y species results in a greater charge transfer away from the Mo than in MoS_2 and a corresponding BE increase from that of MoS_2 in the Mo 3d core level, as is observed in this work. In contrast, removing sulfur from MoS_2 to form a sulfur deficient Mo_xS_y species will result in a decreased BE from that of MoS_2 in the Mo 3d core level as is observed in our previous work.[40]

Up to this point, the sample was exposed to air in between each XPS measurement, in the same way the MoS_2 flakes were in between lithographic contact formation steps. In contrast, all subsequent Ti deposition steps and corresponding XPS were performed *in situ* without breaking vacuum to exclude the effects of air exposure on the Ti/MoS_2 interface chemistry. Previous work has shown the supply of background gases to the MoS_2 surface in HV (i.e., in an elastomer sealed deposition tool) is sufficient to completely oxidize Ti throughout deposition, resulting in a 100% TiO_2 film.[40] However, a more recent study showed that the concentration of oxygen incorporated into a Ti contact during deposition in HV depends significantly on the deposition rate and deposition chamber base pressure.[49] If Ti is completely oxidized during the deposition in this work, then the MoO_3 formed during the O_2 plasma will remain unperturbed by the Ti deposition. Conversely, if the Ti is only partially oxidized during the deposition in this work, any metallic Ti that does not react with background gases will scavenge oxygen from the MoO_3. Therefore, performing the Ti depositions and subsequent XPS *in situ* is critical to accurately characterizing the interface chemistry evolution during Ti deposition on O_2 plasma-treated MoS_2 in this work.

After 1 nm Ti deposition, MoO_x is detected in a mixture of Mo^{5+}, Mo^{3+}, and Mo^{1+} oxidation states in the corresponding Mo 3d core level spectrum (231.4, 229.5, and 228.9 eV, respectively), indicating a significant amount of MoO_x, which is initially present entirely in the Mo^{6+} oxidation state, is reduced by Ti. In addition, 1 nm Ti completely reduces

DOI: 10.1021/acsaelm.8b00059
ACS Appl. Electron. Mater. 2019, 1, 210−219

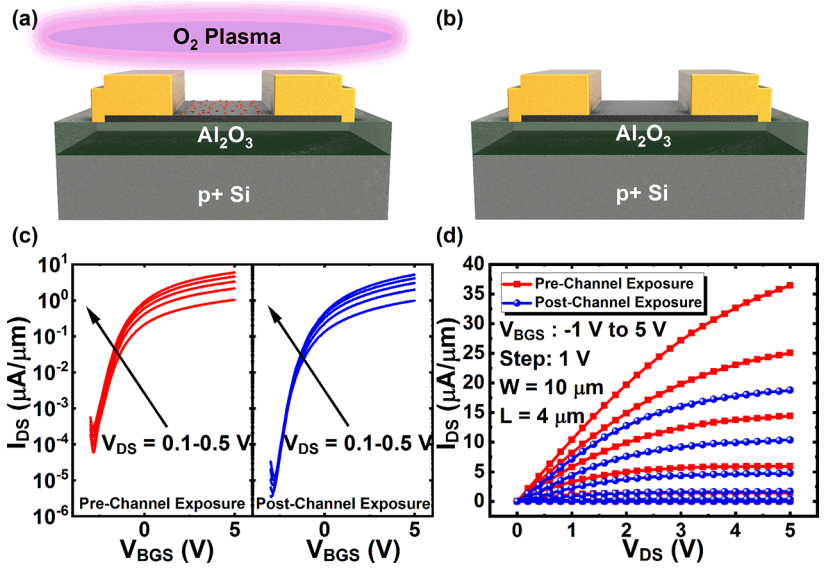

Figure 4. (a) Graphic illustrating O_2 plasma exposure at the exposed channel area and (b) the back-gate MoS_2 FET after channel exposure. (c) Comparison of transfer curves and (d) output characteristics of the same BG MoS_2 FET before and after channel exposure, demonstrating the impact of photoresist residue at the MoS_2 channel region on device performance.

MoS_xO_y, forming TiS_x (228.9 eV in the corresponding S $2p_{3/2}$ spectrum) as a byproduct. After Ti deposition to a thickness of 5 nm, the Mo^{5+} chemical state falls below the limit of detection, and the Mo^{1+} chemical state intensity increases in the corresponding Mo 3d spectrum, which indicates MoO_x is reduced further with increasing Ti film thickness. The MoS_2 chemical states shift 0.3 eV to higher BE after 5 nm Ti deposition compared with that detected after O_2 plasma corresponding with a 0.3 eV Fermi level shift toward the E_C edge.

The Ti 2p core level spectra obtained after Ti deposition to total thicknesses of 1 and 5 nm are shown in Figure 3b. Metallic Ti is below the limit of XPS detection up to a film thickness of 5 nm, which indicates a Ti contact to O_2 plasma-treated MoS_2 is primarily composed of Ti−O and Ti−S bonds. As previously mentioned, a high-quality electron contact to MoS_2 is achieved by treating the contact regions with O_2 plasma and subsequently metallizing with Ti/Au. This indicates Ti reduces MoO_x and forms TiO_x during deposition, which mitigates the hole doping effects of MoO_x and dramatically enhances electron injection into MoS_2 via the deliberately formed TiO_x interlayer.

The presence of resist residue on MoS_2 after development is substantiated by chemical states detected in the corresponding C 1s, O 1s, and N 1s core level spectra consistent with organic species.[50] In addition to forming MoO_x, O_2 plasma removes organic residue according to the decreased intensity of the C═O and C═N chemical states in the corresponding C 1s, N 1s, and O 1s spectra (Figure S5). After Ti deposition, the intensities of chemical states in the corresponding C 1s, O 1s, and N 1s spectra attributed to organic residue decrease more than the expected attenuation of a 1 or 5 nm thick Ti overlayer. This suggests Ti also cleans the interface by scavenging residual organics.[51−53] The evolution of the O 1s, N 1s, and C 1s chemical states throughout the experiment is discussed in greater detail in the Supporting Information.

The reaction mechanism and corresponding electronic effects proposed here rationalize the 0.3 eV Fermi level shift toward the E_C edge detected after 5 nm Ti deposition and the high-performance n-type contact behavior observed in Figure 1d. The enhanced carrier injection accompanying the formation of TiO_x is likely due to a low E_C offset of TiO_2 with MoS_2 as has been demonstrated by Kaushik et al. with an atomic layer deposited (ALD) ultrathin TiO_2 interfacial layer.[40,54] The removal of organic residue along with the Ti scavenging effect demonstrates the dual purpose of the short O_2 plasma exposure prior to contact metal deposition to form high performance n-type contacts on MoS_2.

After the metal deposition and lift-off process, it is intuitive to presume the back-gate MoS_2 FETs would have substantial (at least monolayer concentration) photoresist residue, as well as other adsorbents,[55] on the exposed top channel surface similar to the contact areas. Previous investigations on MoS_2 and graphene involved the use of an anneal to drive off surface contaminants from the channel surface.[31,56] While an anneal potentially affects all device surfaces and interfaces, often convoluting the effects of the anneal in terms of the $I-V$ response,[57] the after effects of the O_2 plasma exposure are more constrained.

To investigate the impact of the channel surface residue on the device performance, without a severe impact on other surfaces and interfaces, the BG MoS_2 FETs were electrically characterized before and after a 5 s O_2 plasma exposure at the channel as shown in Figure 4a,b. The initial transfer curves prior to exposure in Figure 4c demonstrate an OFF current of $\sim 6 \times 10^{-5}$ μA/μm at a V_{DS} of 0.1 V. There is also a negative shift in the threshold voltage (V_T) with increasing drain voltage (V_{DS}) as has been observed in other works on BG MoS_2 FETs.[4,58] This suggests that surface adsorbents can act as charge traps for carriers in the MoS_2 channel as has been suggested in previous reports.[59] After the O_2 plasma exposure, the transfer curves, under the same measurement parameters, demonstrate a lower OFF current of $\sim 4 \times 10^{-6}$ μA/μm at a V_{DS} of 0.1 V as well as no V_T shift with increasing V_{DS}. The higher OFF current combined with the negative ΔV_T shift with increasing V_{DS} prior to exposure suggests the surface contaminants on the top MoS_2 surface may constitute a net positive charge, acting as a n-type dopant. After O_2 plasma

DOI: 10.1021/acsaelm.8b00059
ACS Appl. Electron. Mater. 2019, 1, 210−219

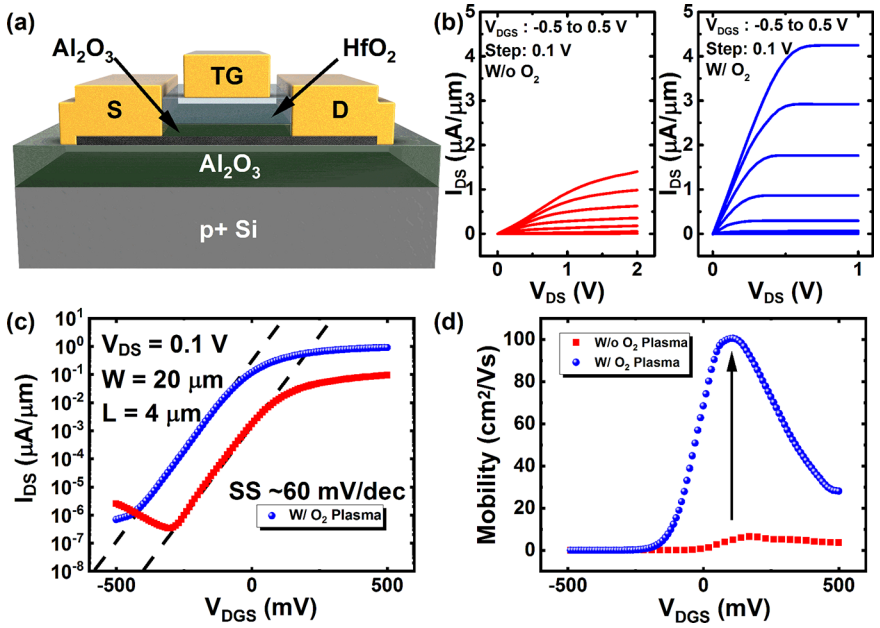

Figure 5. (a) Graphic cross section of a dual-gate (DG) MoS_2 FET with $HfO_2/Al_2O_3/MoS_2/Al_2O_3$ gate stack (W = 20 μm, L = 4 μm). (b) Comparison of output characteristics of DG MoS_2 FETs without O_2 plasma exposure (red) and with O_2 plasma exposure (blue), with the latter demonstrating high performance and linear $I_{DS}-V_{DS}$. (c) Comparison of transfer curves of DG MoS_2 FETs demonstrating a similar, near-ideal SS of ~60 mV/dec with over an order of magnitude increase in ON current for device with O_2 plasma exposure at the contacts. (d) Comparison of field effect mobility demonstrates an increase of ~15× due to a reduction in contact resistance of ~20× because of high quality contact formation in the contact regions.

exposure there is a positive ΔV_T shift, suggesting the elimination of the positive charge at the exposed MoS_2 surface. Furthermore, although there appears to be no change in the ON current of the transfer curves after the O_2 plasma exposure, the output characteristics in Figure 4d show a reduction in saturation current after exposure. This would indicate that the positively charged contaminants on MoS_2 induce a slight excess in electron carrier generation (consistent with FLP at the E_C edge in Figure 3c), in a similar way to the impact of fixed positive oxide charge for high-k dielectrics deposited on MoS_2.[60,61]

Yet a recent study by Liang et al., where post-lithography PMMA residue is removed from MoS_2 and WSe_2 BG FETs' channel surface using an AFM tip, suggests a similar, albeit opposite trend.[19] Their electrical measurements demonstrate a negative ΔV_T shift and an increase in I_{ON} current after residue removal, suggesting the PMMA residue acts as a p-type dopant. Two possible conclusions can be inferred due to the different nature of residue removal in their study and ours: either different resists can act as either n-type (this study) or p-type (Liang et al.) dopants, or the introduction of MoO_x (itself p-type) as a result of O_2 plasma exposure is responsible for the positive ΔV_T shift observed in this study. Studies comparing MoS_2 device behavior before and after O_2 plasma exposure support the latter conclusion rather than the former.[23,24] The simultaneous removal of resist residue and introduction of MoO_x makes it difficult to definitively conclude the dominant mechanism behind the positive ΔV_T shift and reduction in I_{OFF}.

While the channel exposure did improve the device performance, and removed the residue as demonstrated in Figure 2, the nature of the photoresist residue on the channel and its effect on $I-V$ characteristics of BG MoS_2 FETs are convoluted by the introduction of MoO_x. For the purposes of top-gate fabrication it may also influence the formation of S−O bonds during surface functionalization.[32,33] But the removal of surface contaminants is still warranted and can be done *in situ* with a UHV anneal, instead of O_2 plasma, prior to functionalization treatment and high-κ dielectric deposition as described in our earlier work on top-gate, high-κ dielectrics on MoS_2, among others.[28,31,62] Comparisons between dual-gate MoS_2 FETs with and without O_2 plasma exposure solely at the contacts are desirable to demonstrate the plasma treatment's affect on critical device parameters such as mobility.

To help articulate the critical impact of the O_2 plasma clean on overall device performance, the top-gate (TG) stack formation described in the Experimental Section was implemented for multiple BG MoS_2 FETs. For proper comparison, one set of devices had O_2 plasma exposure at the contacts and the other did not, with all other fabrication variables kept the same. The final dual-gate (DG) MoS_2 FET structure had a sub-10 nm high-κ dielectric TG bilayer (Al_2O_3/HfO_2) as shown in Figure 5a. To take advantage of the DG structure, both the TG and BG were simultaneously swept (V_{DGS} = dual-gate sweep) for better electrostatic control of the MoS_2 channel.[34,35] It should be noted that the DG sweep effectively neutralizes the impact of charge traps on the SS (as demonstrated in Figures 2c and 3a of our previous study[35]). Two DG MoS_2 FETs with similar MoS_2 flake thickness and active device areas were chosen and compared in terms of their electrical performance (see Figure S6 for more details). Comparing the output characteristics in Figure 5b, the set without O_2 plasma (red) shows nonlinearity as opposed to the one with O_2 plasma treated contacts (blue). This comparison demonstrates that (even with a 300 °C UHV anneal as well as the thermal heating resulting from the ALD at 200 °C) what the contacts experience during the TG stack formation may

DOI: 10.1021/acsaelm.8b00059
ACS Appl. Electron. Mater. 2019, 1, 210−219

not be enough to completely neutralize the contaminants that are trapped at the contact metal/MoS_2 interface. Major improvements in the transfer curves in Figure 5c are also observed. At a V_{DS} of 0.1 V, both devices demonstrate a near-ideal SS of ∼60 mV/dec with a DG sweep, but a drastic difference in ON current is observed. It should be noted that the V_T difference observed in Figure 5c is due to device to device variability and not a result of the O_2 plasma clean at the contacts. The DG MoS_2 FET with O_2 plasma exposure at the contacts demonstrates an ON current of $\sim 1.1 \times 10^0$ μA/μm compared to $\sim 9.3 \times 10^{-2}$ μA/μm (taken at $V_{OD} = V_G - V_T$ = 0.4 V) for device without O_2 plasma exposure—which is over an order of magnitude increase due to high quality n-type contacts. Because the SS values of both devices are approximately the same, a proper comparison between mobility values can be made based solely on the difference in device contact quality.

The field effect mobility (μ_{FE}) extraction, done using the conventional equation of $\mu_{FE} = g_m(L/W)(1/C_{OX}V_{DS})$, with the capacitance value (C_{OX}) taken to be ∼1.47 μF/cm^2, is compared in Figure 5d. The bottom-gate oxide capacitance ($C_{BOX} \approx 0.65$ μF/cm^2) was extracted using a standard p-Si/Al_2O_3/Ti/Au capacitor structure, while the top-gate oxide capacitance ($C_{TOX} \approx 0.82$ μF/cm^2) was extracted using a split-CV methodology as discussed our previous studies.[62,63] The total capacitance value ($C_{OX} = C_{BOX} + C_{TOX}$) was calculated as two dielectric capacitors in parallel.[34] The μ_{FE} increases ∼15× after O_2 plasma exposure from ∼6.5 to ∼100 cm^2/V·s. This major enhancement is a result of the high-quality contacts due to O_2 plasma exposure. Yet there are still limitations due to the nature of the MoS_2 which can have high and variable impurity concentrations.[46]

The contact resistance (R_C) alone can effectively mask the true mobility, which can be extracted along with the R_C itself using the *Y*-function method.[64] The method used for R_C extraction involves several equations: $Y = I_{DS}/g_m^{1/2} = [(W/L)(\mu_0 C_{OX} V_{DS})]^{1/2}(V_{GS} - V_T)$, $\theta = [(I_{DS}/g_m(V_{GS} - V_T)) - 1]/(V_{GS} - V_T)$, and $\theta = \theta_o + R_C C_{OX} \mu_0 W/L$, where μ_0 is the intrinsic carrier mobility, θ is the mobility degradation factor, and θ_0 is the intrinsic degradation factor (assumed to be negligible due to the significant contribution to θ from R_C as compared to θ_0).[65] The *Y*-function method is an excellent technique because it provides a more realistic R_C value, does not require additional test structures beyond the FET, and requires a limited number of parameters on which results have a weak dependence. The DG MoS_2 FET without O_2 plasma clean demonstrates a *Y*-function extracted R_C of ∼20.2 kΩ·μm compared to ∼1 kΩ·μm for the device with O_2 plasma, resulting in high quality contacts as shown in Figure S7a. This trend holds for multiple DG MoS_2 FETs as shown in Figure S7b. Furthermore, the intrinsic carrier mobility (μ_0), which was extracted along with the R_C, for the DG MoS_2 FET with O_2 plasma exposure at the contacts is ∼310 cm^2/V·s, suggesting that further improvements in the quality of TMD materials are necessary.

A low Schottky barrier height (SBH) is a good indicator of a R_C that is low and linear. The SBH extraction was done assuming conventional thermionic emission theory, where slopes of curves in Figure S8 in the high-temperature region are analyzed. Care was taken to ensure that the extracted barrier height was taken where the effective barrier height is linearly responding to changes in the V_{GS}.[12] The point where Φ_{SBH} deviates from the linear trend is where tunneling current ($I_{tunneling}$) begins to take effect as discussed in greater detail elsewhere[66,67] (also see further clarification in the Supporting Information). The SBH extraction (see Figure S8) demonstrates a low SBH of 86 ± 12.8 meV, comparable to other works with a TiO_2 interfacial layer on MoS_2.[54,68] The most recent work by Kim et al. includes a SBH extracted value of 107 meV for a Ti/TiO_2/MoS_2 contact, although the role of photoresist residue is not accounted for and a different origin for the FLP is presented.[68] Yet the observed FLP near the E_C edge of MoS_2 and a low SBH are consistent with this work (Figures S4 and S8). This would indicate that although the nature of FLP for metal contacts on TMDs may be consistent across the literature, the exact origin is still a topic that requires further investigation and debate as reiterated in a recent review of contacts for 2D materials by Schulman et al.[69]

IV. CONCLUSION

This work investigated the use of an O_2 plasma clean prior contact metal deposition to achieve a high-quality contact interface for MoS_2 devices. Topographical, interfacial, and electrical test studies show that photoresist residue, if not properly neutralized, can play a significant role in affecting the electrical properties of MoS_2. The origin of the observed Fermi level pinning near the conduction band edge of MoS_2 appears to result from the photoresist residue itself. The removal of organic residue—combined with the formation of a high-performance n-type TiO_x/MoS_2 contact interface due to oxygen scavenging by Ti—demonstrates the dual use of O_2 plasma exposure. Furthermore, a comparison between DG MoS_2 FETs with and without O_2 plasma exposure demonstrates an ∼15× improvement in mobility and an ∼20× reduction in contact resistance due to the formation of higher quality contacts with O_2 plasma. The results show that the effects of contaminants left over from the device fabrication processes can significantly hamper MoS_2 transistor performance if not properly eliminated. Further reductions in contact resistance may be possible with the use of semiconductor grade, low impurity TMD materials which could further improve transistor performance.

■ ASSOCIATED CONTENT

Supporting Information

The Supporting Information is available free of charge on the ACS Publications website at DOI: 10.1021/acsaelm.8b00059.

Thorough process flow diagram for contact formation for MoS_2 FETs (Figure S1); consistency of output characteristics of multiple MoS_2 FETs (Figure S2); effects of O_2 plasma exposure on MoS_2 flake thickness (Figure S3); determination of valence band edge and band alignment of MoS_2 (Figure S4); O 1s, N 1s, and C 1s core level spectra (Figure S5); active device areas of comparable dual-gate MoS_2 FETs (Figure S6); *Y*-function extracted contact resistance of multiple MoS_2 FETs (Figure S7); Schottky barrier height extraction of MoS_2 FETs (Figure S8) (PDF)

■ AUTHOR INFORMATION

Corresponding Author

*E-mail: chadwin.young@utdallas.edu (C.D.Y.).

ORCID

Peng Zhao: 0000-0002-3530-6400

Christopher L. Hinkle: 0000-0002-5485-6600

DOI: 10.1021/acsaelm.8b00059
ACS Appl. Electron. Mater. 2019, 1, 210−219

Robert M. Wallace: 0000-0001-5566-4806
Chadwin D. Young: 0000-0003-0690-7423

Notes

The authors declare no competing financial interest.

■ ACKNOWLEDGMENTS

This work was supported in part by the US/Ireland R&D Partnership (UNITE) under the NSF Award ECCS-1407765/SFI Award (13/US/I2862) and the NSF CAREER Award ECCS-1653343. This work was also supported in part by Semiconductor Research Corporation (SRC) as the NEW-LIMITS Center, NIST, through Award 70NANB17H041 and by SFI through the IvP award (15/IA/3131).

■ REFERENCES

(1) Das, S.; Prakash, A.; Salazar, R.; Appenzeller, J. Toward Low-Power Electronics: Tunneling Phenomena in Transition Metal Dichalcogenides. *ACS Nano* **2014**, *8* (2), 1681−1689.
(2) Jariwala, D.; Sangwan, V. K.; Lauhon, L. J.; Marks, T. J.; Hersam, M. C. Emerging Device Applications for Semiconducting Two-Dimensional Transition Metal Dichalcogenides. *ACS Nano* **2014**, *8* (2), 1102−1120.
(3) Radisavljevic, B.; Radenovic, A.; Brivio, J.; Giacometti, V.; Kis, A. Single-Layer MoS_2 Transistors. *Nat. Nanotechnol.* **2011**, *6* (3), 147−150.
(4) Liu, H.; Neal, A. T.; Ye, P. D. Channel Length Scaling of MoS_2 MOSFETs. *ACS Nano* **2012**, *6* (10), 8563−8569.
(5) Tsai, M.-L.; Li, M.-Y.; Retamal, J. R. D.; Lam, K.-T.; Lin, Y.-C.; Suenaga, K.; Chen, L.-J.; Liang, G.; Li, L.-J.; He, J.-H. Single Atomically Sharp Lateral Monolayer P-n Heterojunction Solar Cells with Extraordinarily High Power Conversion Efficiency. *Adv. Mater.* **2017**, *29* (32), 1701168.
(6) Tsai, D.-S.; Liu, K.-K.; Lien, D.-H.; Tsai, M.-L.; Kang, C.-F.; Lin, C.-A.; Li, L.-J.; He, J.-H. Few-Layer MoS_2 with High Broadband Photogain and Fast Optical Switching for Use in Harsh Environments. *ACS Nano* **2013**, *7* (5), 3905−3911.
(7) Kappera, R.; Voiry, D.; Yalcin, S. E.; Branch, B.; Gupta, G.; Mohite, A. D.; Chhowalla, M. Phase-Engineered Low-Resistance Contacts for Ultrathin MoS_2 Transistors. *Nat. Mater.* **2014**, *13* (12), 1128−1134.
(8) Chang, H. Y.; Zhu, W.; Akinwande, D. On the Mobility and Contact Resistance Evaluation for Transistors Based on MoS_2 or Two-Dimensional Semiconducting Atomic Crystals. *Appl. Phys. Lett.* **2014**, *104* (11), 113504.
(9) McDonnell, S.; Addou, R.; Buie, C.; Wallace, R. M.; Hinkle, C. L. Defect-Dominated Doping and Contact Resistance in MoS_2. *ACS Nano* **2014**, *8* (3), 2880−2888.
(10) Durán Retamal, J. R.; Periyanagounder, D.; Ke, J.-J.; Tsai, M.-L.; He, J.-H. Charge Carrier Injection and Transport Engineering in Two-Dimensional Transition Metal Dichalcogenides. *Chem. Sci.* **2018**, *9* (40), 7727−7745.
(11) Akinwande, D.; Petrone, N.; Hone, J. Two-Dimensional Flexible Nanoelectronics. *Nat. Commun.* **2014**, *5* (1), 5678.
(12) Das, S.; Chen, H. Y.; Penumatcha, A. V.; Appenzeller, J. High Performance Multilayer MoS_2 Transistors with Scandium Contacts. *Nano Lett.* **2013**, *13* (1), 100−105.
(13) Neal, A. T.; Liu, H.; Gu, J. J.; Ye, P. D. Metal Contacts to MoS_2: A Two-Dimensional Semiconductor. In *Device Research Conference - Conference Digest, DRC*; IEEE: 2012; pp 65−66.
(14) English, C. D.; Shine, G.; Dorgan, V. E.; Saraswat, K. C.; Pop, E. Improved Contacts to MoS_2 Transistors by Ultra-High Vacuum Metal Deposition. *Nano Lett.* **2016**, *16* (6), 3824−3830.
(15) Smyth, C. M.; Addou, R.; McDonnell, S.; Hinkle, C. L.; Wallace, R. M. Contact Metal−MoS_2 Interfacial Reactions and Potential Implications on MoS_2 -Based Device Performance. *J. Phys. Chem. C* **2016**, *120* (27), 14719−14729.
(16) Kwon, J.; Lee, J.-Y.; Yu, Y.-J.; Lee, C.-H.; Cui, X.; Hone, J.; Lee, G.-H. Thickness-Dependent Schottky Barrier Height of MoS_2 Field-Effect Transistors. *Nanoscale* **2017**, *9* (18), 6151−6157.
(17) Pirkle, A.; Chan, J.; Venugopal, A.; Hinojos, D.; Magnuson, C. W.; McDonnell, S.; Colombo, L.; Vogel, E. M.; Ruoff, R. S.; Wallace, R. M. The Effect of Chemical Residues on the Physical and Electrical Properties of Chemical Vapor Deposited Graphene Transferred to SiO_2. *Appl. Phys. Lett.* **2011**, *99* (12), 122108.
(18) Chan, J.; Venugopal, A.; Pirkle, A.; McDonnell, S.; Hinojos, D.; Magnuson, C. W.; Ruoff, R. S.; Colombo, L.; Wallace, R. M.; Vogel, E. M. Reducing Extrinsic Performance-Limiting Factors in Graphene Grown by Chemical Vapor Deposition. *ACS Nano* **2012**, *6* (4), 3224−3229.
(19) Liang, J.; Xu, K.; Toncini, B.; Bersch, B.; Jariwala, B.; Lin, Y.-C.; Robinson, J.; Fullerton-Shirey, S. K. Impact of Post-Lithography Polymer Residue on the Electrical Characteristics of MoS_2 and WSe_2 Field Effect Transistors. *Adv. Mater. Interfaces* **2018**, 1801321.
(20) Tiwari, C. S.; Lim, Y. S.; Fulton, R.; Srinivasan, J.; Gisinger, M.; Flynn, P.; Mak, L. H. Characterization of the Descum Process for Various Silicon Substrates Doping. *ECS Trans.* **2013**, *58* (6), 251−259.
(21) Yang, W.; Sun, Q.-Q.; Geng, Y.; Chen, L.; Zhou, P.; Ding, S.-J.; Zhang, D. W. The Integration of Sub-10 nm Gate Oxide on MoS_2 with Ultra Low Leakage and Enhanced Mobility. *Sci. Rep.* **2015**, *5* (1), 11921.
(22) Zhu, H.; Qin, X.; Cheng, L.; Azcatl, A.; Kim, J.; Wallace, R. M. Remote Plasma Oxidation and Atomic Layer Etching of MoS_2. *ACS Appl. Mater. Interfaces* **2016**, *8* (29), 19119−19126.
(23) Jadwiszczak, J.; O'Callaghan, C.; Zhou, Y.; Fox, D. S.; Weitz, E.; Keane, D.; Cullen, C. P.; O'Reilly, I.; Downing, C.; Shmeliov, A.; Maguire, P.; Gough, J. J.; McGuinness, C.; Ferreira, M. S.; Bradley, A. L.; Boland, J. J.; Duesberg, G. S.; Nicolosi, V.; Zhang, H. Oxide-Mediated Recovery of Field-Effect Mobility in Plasma-Treated MoS_2. *Sci. Adv.* **2018**, *4* (3), No. eaao5031.
(24) Nan, H.; Wu, Z.; Jiang, J.; Zafar, A.; You, Y.; Ni, Z. Improving the Electrical Performance of MoS_2 by Mild Oxygen Plasma Treatment. *J. Phys. D: Appl. Phys.* **2017**, *50* (15), 154001.
(25) Li, H.; Wu, J.; Huang, X.; Lu, G.; Yang, J.; Lu, X.; Xiong, Q.; Zhang, H. Rapid and Reliable Thickness Identification of Two-Dimensional Nanosheets Using Optical Microscopy. *ACS Nano* **2013**, *7* (11), 10344−10353.
(26) 2D Semiconductors; http://www.2dsemiconductors.com.
(27) Singh, A. K.; Hennig, R. G.; Davydov, A. V.; Tavazza, F. Al_2O_3 as a Suitable Substrate and a Dielectric Layer for n-Layer MoS_2. *Appl. Phys. Lett.* **2015**, *107* (5), 053106.
(28) Bolshakov, P.; Zhao, P.; Azcatl, A.; Hurley, P. K.; Wallace, R. M.; Young, C. D. Improvement in Top-Gate MoS_2 Transistor Performance Due to High Quality Backside Al_2O_3 Layer. *Appl. Phys. Lett.* **2017**, *111* (3), 032110.
(29) Photoresist AZ nLof 2020 Photoresists MicroChemicals GmbH; https://www.microchemicals.com/products/photoresists/az_nlof_2020.html.
(30) McDonnell, S.; Dong, H.; Hawkins, J. M.; Brennan, B.; Milojevic, M.; Aguirre-Tostado, F. S.; Zhernokletov, D. M.; Hinkle, C. L.; Kim, J.; Wallace, R. M. Interfacial Oxide Re-Growth in Thin Film Metal Oxide III-V Semiconductor Systems. *Appl. Phys. Lett.* **2012**, *100* (14), 141606.
(31) Zhao, P.; Azcatl, A.; Bolshakov, P.; Moon, J.; Hinkle, C. L.; Hurley, P. K.; Wallace, R. M.; Young, C. D. Effects of Annealing on Top-Gated MoS_2 Transistors with HfO_2 Dielectric. *J. Vac. Sci. Technol., B: Nanotechnol. Microelectron.: Mater., Process., Meas., Phenom.* **2017**, *35* (1), 01A118.
(32) Azcatl, A.; McDonnell, S.; Santosh, K. C.; Peng, X.; Dong, H.; Qin, X.; Addou, R.; Mordi, G. I.; Lu, N.; Kim, J.; Kim, M. J.; Cho, K.; Wallace, R. M. MoS_2 Functionalization for Ultra-Thin Atomic Layer Deposited Dielectrics. *Appl. Phys. Lett.* **2014**, *104* (11), 111601.
(33) Azcatl, A.; Kc, S.; Peng, X.; Lu, N.; McDonnell, S. S.; Qin, X.; De Dios, F.; Addou, R.; Kim, J.; Kim, M. J.; Cho, K.; Wallace, R. M.

HfO_2 on UV-O_3 Exposed Transition Metal Dichalcogenides: Interfacial Reactions Study. *2D Mater.* **2015**, *2* (1), 014004.
(34) Kim, J. S.; Jeon, P. J.; Lee, J.; Choi, K.; Lee, H. S.; Cho, Y.; Lee, Y. T.; Hwang, D. K.; Im, S. Dual Gate Black Phosphorus Field Effect Transistors on Glass for NOR Logic and Organic Light Emitting Diode Switching. *Nano Lett.* **2015**, *15* (9), 5778−5783.
(35) Bolshakov, P.; Khosravi, A.; Zhao, P.; Hurley, P. K.; Hinkle, C. L.; Wallace, R. M.; Young, C. D. Dual-Gate MoS_2 Transistors with Sub-10 nm Top-Gate High-k Dielectrics. *Appl. Phys. Lett.* **2018**, *112* (25), 253502.
(36) Wallace, R. M. In-Situ Studies of Interfacial Bonding of High-k Dielectrics for CMOS Beyond 22nm. *ECS Trans.* **2008**, *16* (5), 255−271.
(37) Smyth, C. M.; Addou, R.; McDonnell, S.; Hinkle, C. L.; Wallace, R. M. WSe_2 -Contact Metal Interface Chemistry and Band Alignment under High Vacuum and Ultra High Vacuum Deposition Conditions. *2D Mater.* **2017**, *4* (2), 025084.
(38) ASTM E2108-00; *Standard Practice for Calibration of the Electron Binding-Energy Scale of an X-Ray Photoelectron Spectrometer*; ASTM International: West Conshohocken, PA, 2000; p E2108-00.
(39) Herrera-Gómez, A.; Hegedus, A.; Meissner, P. L. Chemical Depth Profile of Ultrathin Nitrided SiO_2 Films. *Appl. Phys. Lett.* **2002**, *81* (6), 1014−1016.
(40) McDonnell, S.; Smyth, C.; Hinkle, C. L.; Wallace, R. M. MoS_2-Titanium Contact Interface Reactions. *ACS Appl. Mater. Interfaces* **2016**, *8* (12), 8289−8294.
(41) McDonnell, S.; Azcatl, A.; Addou, R.; Gong, C.; Battaglia, C.; Chuang, S.; Cho, K.; Javey, A.; Wallace, R. M. Hole Contacts on Transition Metal Dichalcogenides: Interface Chemistry and Band Alignments. *ACS Nano* **2014**, *8* (6), 6265−6272.
(42) Chuang, S.; Battaglia, C.; Azcatl, A.; McDonnell, S.; Kang, J. S.; Yin, X.; Tosun, M.; Kapadia, R.; Fang, H.; Wallace, R. M.; Javey, A. MoS_2 P-Type Transistors and Diodes Enabled by High Work Function MoO_x Contacts. *Nano Lett.* **2014**, *14* (3), 1337−1342.
(43) Santosh, K. C.; Longo, R. C.; Addou, R.; Wallace, R. M.; Cho, K. Electronic Properties of MoS_2/MoO_x Interfaces: Implications in Tunnel Field Effect Transistors and Hole Contacts. *Sci. Rep.* **2016**, *6* (1), 33562.
(44) Liu, H.; Si, M.; Deng, Y.; Neal, A. T.; Du, Y.; Najmaei, S.; Ajayan, P. M.; Lou, J.; Ye, P. D. Switching Mechanism in Single-Layer Molybdenum Disulfide Transistors: An Insight into Current Flow across Schottky Barriers. *ACS Nano* **2014**, *8* (1), 1031−1038.
(45) Kim, S. Y.; Park, S.; Choi, W. Variability of Electrical Contact Properties in Multilayer MoS_2 Thin-Film Transistors. *Appl. Phys. A: Mater. Sci. Process.* **2014**, *117* (2), 761−766.
(46) Addou, R.; McDonnell, S.; Barrera, D.; Guo, Z.; Azcatl, A.; Wang, J.; Zhu, H.; Hinkle, C. L.; Quevedo-Lopez, M.; Alshareef, H. N.; Colombo, L.; Hsu, J. W. P.; Wallace, R. M. Impurities and Electronic Property Variations of Natural MoS_2 Crystal Surfaces. *ACS Nano* **2015**, *9* (9), 9124−9133.
(47) Kim, C.; Moon, I.; Lee, D.; Choi, M. S.; Ahmed, F.; Nam, S.; Cho, Y.; Shin, H.-J.; Park, S.; Yoo, W. J. Fermi Level Pinning at Electrical Metal Contacts of Monolayer Molybdenum Dichalcogenides. *ACS Nano* **2017**, *11* (2), 1588−1596.
(48) Chemical Bonding; www.chemhume.co.uk.
(49) Freedy, K. M.; Giri, A.; Foley, B. M.; Barone, M. R.; Hopkins, P. E.; McDonnell, S. Titanium Contacts to Graphene: Process-Induced Variability in Electronic and Thermal Transport. *Nanotechnology* **2018**, *29* (14), 145201.
(50) Introduction to DNQ-Novolac Resists - Henderson Research Group; https://sites.google.com/site/hendersonresearchgroup/helpful-primers-introductions/intro-to-dnq-novolac-resists.
(51) Venugopal, A. Effect of Contacts, Graphene Type and Underlying Substrate on the Transport Properties of Graphene. Ph.D. Dissertation, The University of Texas at Dallas, Richardson, TX, 2012.
(52) Colombo, L.; Wallace, R. M.; Ruoff, R. S. Graphene Growth and Device Integration. *Proc. IEEE* **2013**, *101* (7), 1536−1556.
(53) Joiner, C. A.; Roy, T.; Hesabi, Z. R.; Chakrabarti, B.; Vogel, E. M. Cleaning Graphene with a Titanium Sacrificial Layer. *Appl. Phys. Lett.* **2014**, *104* (22), 223109.
(54) Kaushik, N.; Karmakar, D.; Nipane, A.; Karande, S.; Lodha, S. Interfacial N-Doping Using an Ultrathin TiO_2 Layer for Contact Resistance Reduction in MoS_2. *ACS Appl. Mater. Interfaces* **2016**, *8* (1), 256−263.
(55) Sangwan, V. K.; Arnold, H. N.; Jariwala, D.; Marks, T. J.; Lauhon, L. J.; Hersam, M. C. Low-Frequency Electronic Noise in Single-Layer MoS_2 Transistors. *Nano Lett.* **2013**, *13* (9), 4351−4355.
(56) Pirkle, A. R.; Chabal, Y. J.; Colombo, L.; Wallace, R. M. In-Situ Studies of High-κ Dielectrics for Graphene-Based Device. *ECS Trans.* **2009**, *19* (5), 215−224.
(57) Namgung, S. D.; Yang, S.; Park, K.; Cho, A. J.; Kim, H.; Kwon, J. Y. Influence of Post-Annealing on the off Current of MoS_2 Field-Effect Transistors. *Nanoscale Res. Lett.* **2015**, *10* (1), 1−6.
(58) Xu, J.; Chen, L.; Dai, Y. W.; Cao, Q.; Sun, Q. Q.; Ding, S. J.; Zhu, H.; Zhang, D. W. A Two-Dimensional Semiconductor Transistor with Boosted Gate Control and Sensing Ability. *Sci. Adv.* **2017**, *3* (5), No. e1602246.
(59) Illarionov, Y. Y.; Smithe, K. K. H.; Waltl, M.; Knobloch, T.; Pop, E.; Grasser, T. Improved Hysteresis and Reliability of MoS_2 Transistors with High-Quality CVD Growth and Al_2O_3 Encapsulation. *IEEE Electron Device Lett.* **2017**, *38* (12), 1763−1766.
(60) Li, T.; Wan, B.; Du, G.; Zhang, B.; Zeng, Z. Electrical Performance of Multilayer MoS_2 Transistors on High- κ Al_2O_3 Coated Si Substrates. *AIP Adv.* **2015**, *5* (5), 057102.
(61) Na, J.; Joo, M.-K.; Shin, M.; Huh, J.; Kim, J.-S.; Piao, M.; Jin, J.-E.; Jang, H.-K.; Choi, H. J.; Shim, J. H.; Kim, G.-T. Low-Frequency Noise in Multilayer MoS_2 Field-Effect Transistors: The Effect of High-k Passivation. *Nanoscale* **2014**, *6* (1), 433−441.
(62) Zhao, P.; Azcatl, A.; Gomeniuk, Y. Y.; Bolshakov, P.; Schmidt, M.; McDonnell, S. J.; Hinkle, C. L.; Hurley, P. K.; Wallace, R. M.; Young, C. D. Probing Interface Defects in Top-Gated MoS_2 Transistors with Impedance Spectroscopy. *ACS Appl. Mater. Interfaces* **2017**, *9* (28), 24348−24356.
(63) Zhao, P.; Khosravi, A.; Azcatl, A.; Bolshakov, P.; Mirabelli, G.; Caruso, E.; Hinkle, C. L.; Hurley, P. K.; Wallace, R. M.; Young, C. D. Evaluation of Border Traps and Interface Traps in HfO_2/MoS_2 Gate Stacks by Capacitance−voltage Analysis. *2D Mater.* **2018**, *5* (3), 031002.
(64) Fleury, D.; Cros, A.; Brut, H.; Ghibaudot, G. New Y-Function-Based Methodology for Accurate Extraction of Electrical Parameters on Nano-Scaled MOSFETs. In *IEEE International Conference on Microelectronic Test Structures*; IEEE: 2008; pp 160−165.
(65) Bhattacharjee, S.; Ganapathi, K. L.; Nath, D. N.; Bhat, N. Intrinsic Limit for Contact Resistance in Exfoliated Multilayered MoS_2 FET. *IEEE Electron Device Lett.* **2016**, *37* (1), 119−122.
(66) Appenzeller, J.; Knoch, J.; Bjork, M. T.; Riel, H.; Schmid, H.; Riess, W. Toward Nanowire Electronics. *IEEE Trans. Electron Devices* **2008**, *55* (11), 2827−2845.
(67) Heinze, S.; Tersoff, J.; Martel, R.; Derycke, V.; Appenzeller, J.; Avouris, P. Carbon Nanotubes as Schottky Barrier Transistors. *Phys. Rev. Lett.* **2002**, *89* (10), 106801.
(68) Kim, G.-S.; Kim, S.-H.; Park, J.; Hyun Han, K.; Kim, J.; Yu, H.-Y. Schottky Barrier Height Engineering for Electrical Contacts of Multilayered MoS_2 Transistors with Reduction of Metal-Induced Gap States. *ACS Nano* **2018**, *12* (6), 6292−6300.
(69) Schulman, D. S.; Arnold, A. J.; Das, S. Contact Engineering for 2D Materials and Devices. *Chem. Soc. Rev.* **2018**, *47* (9), 3037−3058.

DOI: 10.1021/acsaelm.8b00059
ACS Appl. Electron. Mater. 2019, 1, 210−219